LASER & PHOTONICS REVIEWS

www.lpr-journal.org

Stable High-Dimensional Weak-Light Soliton Molecules and Their Active Control

*Lu Qin, Chao Hang, Boris A. Malomed, and Guoxiang Huang**

Bound states of solitons, alias soliton molecules (SMs), are well known in 1D systems, while making stable bound states of multidimensional solitons is a challenging problem because of the underlying instabilities. Here, a scheme for the creation of stable (2+1)D and (3+1)D optical SMs in a gas of cold Rydberg atoms is proposed, in which electromagnetically induced transparency (EIT) is induced by a control laser field. It is shown that, through the interplay of the EIT and the strong long-range interaction between the Rydberg atoms, the system gives rise to giant nonlocal Kerr nonlinearity, which in turn supports stable (2+1)D spatial optical SMs, as well as ring-shaped soliton necklaces, including rotating ones. They feature a large size, low generation power, and can be efficiently manipulated by tuning the nonlocality degree of the Kerr nonlinearity. Stable (3+1)D spatiotemporal optical SMs, composed of fundamental or vortex solitons, with low power and ultraslow propagation velocity, can also be generated in the system. These SMs can be stored and retrieved through the switching off and on of the control laser field. The findings reported here suggest applications to data processing and transmission in optical systems.

1. Introduction

Solitons are self-trapped wave packets maintained by the interplay between dispersion (and/or diffraction) and nonlinearity of host media.[1,2] They are ubiquitous in nature, having been discovered in many areas, including hydrodynamics and plasmas,[3] optics,[4–14] Bose–Einstein condensates,[15–18] superconductivity,[19] solid-state physics, magnetic media, etc.[20–22] While in (nearly) integrable systems solitons interact elastically,[1,2] collisions between them in nonintegrable settings exhibit a variety of outcomes, including, in particular, fusion, fission, and annihilation.[23–35] In this context, bound states of solitons[36–46] often referred as soliton molecules (SMs), are objects of great interest, as they demonstrate unique properties and offer various potential applications for working with mode-locked fiber lasers, matter waves, optical microresonators, polariton superfluids, and other physical realizations.[47–79] Especially promising applications of SMs in the area of photonics include the design of new laser schemes, switchers, and data carriers.[55,58,62,77]

Previous studies of SMs were chiefly limited to 1D systems with local nonlinearity, such as temporal SMs in fiber lasers. In such systems, the interaction between solitons in the SM is determined by the overlap of "tails" of the wave functions of adjacent solitons, which rapidly decays as the separation between the solitons increases. As a result, the size of SMs in locally nonlinear media usually does not exceed two or three widths of the single soliton, and they may be readily subject to instability against long-wavelength transverse perturbations when the 1D setting is embedded in the 3D space. In fact, unlike 1D solitons, which are normally stable states, stability of 2D and 3D solitons is a problem as the usual cubic self-focusing gives rise to the critical and supercritical collapse in the 2D and 3D space, respectively,[3,80–83] which makes multidimensional solitons unstable in these simple models. Still more unstable, against spontaneous splitting, are 2D and 3D solitons with embedded vorticity.[84–86] Therefore, identification of physically relevant mechanism for stabilizing fundamental and vortex solitons is a problem of fundamental significance. In recent years, it was addressed in various models, leading to predictions of stable multidimensional solitons in relatively sophisticated settings.[82,86–89] Experimentally, stable 2D spatial solitons were created in an optical medium with cubic-quintic

L. Qin, C. Hang, G. Huang
State Key Laboratory of Precision Spectroscopy
East China Normal University
Shanghai 200062, China
E-mail: gxhuang@phy.ecnu.edu.cn

C. Hang, G. Huang
NYU-ECNU Institute of Physics
New York University at Shanghai
Shanghai 200062, China

C. Hang, G. Huang
Collaborative Innovation Center of Extreme Optics
Shanxi University
Taiyuan, Shanxi 030006, China

L. Qin
Department of Physics
Henan Normal University
Xinxiang 453007, China

B. A. Malomed
Department of Physical Electronics
School of Electrical Engineering
Faculty of Engineering
Tel Aviv University
Ramat Aviv, Tel Aviv 6997801, Israel

B. A. Malomed
Instituto de Alta Investigación
Universidad de Tarapacá
Casilla 7D, Arica1000000, Chile

The ORCID identification number(s) for the author(s) of this article can be found under https://doi.org/10.1002/lpor.202100297

DOI: 10.1002/lpor.202100297

nonlinearity,[90] and in various forms of quasi-soliton "quantum droplets" in BECs.[91–96] As for 2D solitons with embedded vorticity, so far they were experimentally demonstrated only in a transient form, being temporarily stabilized in an optical material with the saturable self-focusing and three-photon absorption.[97]

Another promising possibility is the use of optical media with nonlocal interactions, which make it possible to support stable multidimensional solitons[98–113] and long-range interactions between them.[114,115] The objective of the present work is to elaborate a scenario for the creation of stable 2D and 3D optical SMs in a cold Rydberg atomic gas, under the condition of the electromagnetically induced transparency (EIT).[116] The large electric-dipole moments of Rydberg atoms give rise to strong long-range interactions between them.[117–119] The interplay of Rydberg–Rydberg interactions with EIT gives rise to a giant nonlocal Kerr nonlinearity.[120–123] In this work, we find that the system supports stable 2D spatial optical SMs that can be built of fundamental or vortex solitons, with the size more than six times the soliton's width ($\approx$ 100 μm). Furthermore, the power required to generate SMs is found to be at microwatts, which is, at least, three orders of magnitude smaller than SM-generation power in fiber-laser systems and solid-state media such as, lead glass, where it may be up to several watts;[67–70,75,114] moreover, properties of the Rydberg-EIT medium make it possible to efficiently control the size of SMs by tuning the degree of the nonlocality of the Kerr nonlinearity.

In addition to two-soliton molecules, stable ring-shaped bound states built of several solitons ("necklaces"), fundamental or vortex ones, carrying overall phase circulation, are constructed too, including rotating necklaces.

We also find that stable bound states of fundamental and vortex 3D spatial-temporal solitons, with ultralow propagation velocity ($\approx 10^{-5}\,c$, where c is the light speed in vacuum) and ultralow generation power, can be created by means of an appropriate combination of nonlocal and local Kerr nonlinearities in such a Rydberg gas. An essential asset of the system under the consideration is that it is highly controllable, admitting one to store and retrieve the predicted 3D spatiotemporal SMs with high fidelity by switching the control field off and on. The results reported here suggest the realization of novel SMs at weak-power levels, and implementation of their effective manipulation, with potential applications to optical data processing and transmission.

The following presentation is arranged as follows. In Section 2, we describe the physical model and derive an envelope equation governing the propagation of the probe field. In Section 3, we address the interaction between spatial solitons, formation of SMs, and necklace-shaped bound states, and manipulation with them by adjusting the nonlocal Kerr nonlinearity. The possibilities to create and manipulate stable spatiotemporal SMs are reported in Section 4. The work is summarized in Section 5.

2. The Model

2.1. The Physical Setup

We start by considering a laser-cooled, dilute three-level atomic gas, interacting with a weak probe laser field $\mathbf{E}_p$ with center frequency ω_p (wavenumber $k_p = \omega_p/c$), driving the transition $|1\rangle \leftrightarrow |2\rangle$, and a strong, continuous-wave control laser field $\mathbf{E}_c$

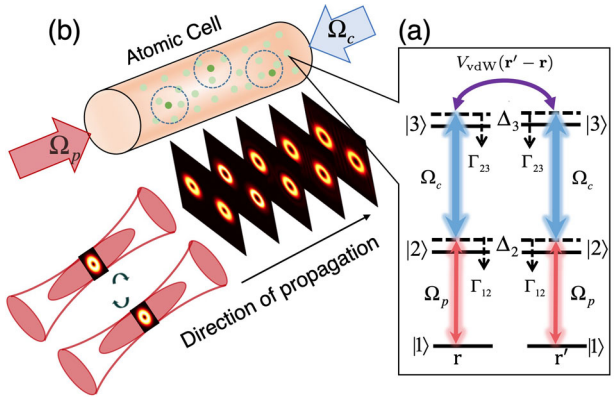

Figure 1. Schematics of the model. a) Energy-level diagram and excitation scheme of two ladder-type three-level atoms. $|1\rangle$, $|2\rangle$, and $|3\rangle$ are respectively the ground, intermediate, and Rydberg states; Γ_{12} and Γ_{23} are respectively decay rates of $|2\rangle$ and $|3\rangle$; Ω_p and Ω_c are respectively half Rabi frequencies of the probe and control laser fields; Δ_2 and Δ_3 are respectively one- and two-photon detunings. The interaction between the two Rydberg atoms is described by the van der Waals potential $V_{vdW}(\mathbf{r}'-\mathbf{r}) = -\hbar C_6/|\mathbf{r}'-\mathbf{r}|^6$. b) Top part: possible experimental geometry. Bottom part: the contactless interaction between two optical vortices, which form a stable vortex molecule.

with frequency ω_c (wavenumber $k_c = \omega_c/c$), driving the transition $|2\rangle \leftrightarrow |3\rangle$; see **Figure 1**a.

Here $|1\rangle$, $|2\rangle$, and $|3\rangle$ denote, respectively, the ground, intermediate, and high-lying Rydberg states; Γ_{12} and Γ_{23} are spontaneous-emission decay rates from $|2\rangle$ to $|1\rangle$ and from $|3\rangle$ to $|2\rangle$, respectively. The interaction between the two Rydberg atoms respectively at positions $\mathbf{r}$ and $\mathbf{r}'$ is described by the van der Waals (vdW) potential

$$V_{vdW} = \hbar V(\mathbf{r}'-\mathbf{r}) \equiv -\frac{\hbar C_6}{|\mathbf{r}'-\mathbf{r}|^6} \tag{1}$$

with C_6 the dispersion coefficient.[117,118] The initial atomic population is prepared in the ground state $|1\rangle$. The total electric-field vector in the system is given by $\mathbf{E} = \mathbf{E}_c + \mathbf{E}_p \equiv \sum_{l=c,p} \mathbf{e}_l \mathcal{E}_l \exp[i(\mathbf{k}_l \cdot \mathbf{r} - \omega_l t)] + \text{c.c.}$, where c.c. stands for the complex conjugate, while $\mathbf{e}_c$ and $\mathbf{e}_p$ ($\mathcal{E}_c$ and $\mathcal{E}_p$) are, respectively, polarization unit vectors (envelopes) of the control and probe fields. To suppress the Doppler effect, the probe and control fields are assumed to counter-propagate along the z-direction, that is, $\mathbf{k}_p = k_p \mathbf{e}_z$ and $\mathbf{k}_c = -k_c \mathbf{e}_z$, with $\mathbf{e}_z$ being the unit vector of the z direction.

The Hamiltonian of the system is given by $\hat{H} = \mathcal{N}_a \int d^3 r \hat{\mathcal{H}}_0(\mathbf{r}, t) + (\mathcal{N}_a/2) \int d^3 r \hat{\mathcal{H}}_1(\mathbf{r}, t)$. Here $d^3 r = dxdydz$, $\mathcal{N}_a$ is atomic density, $\hat{\mathcal{H}}_0(\mathbf{r}, t)$ is the Hamiltonian density describing the atoms and the coupling between the atoms and light fields, $\hat{\mathcal{H}}_1(\mathbf{r}, t)$ is the Hamiltonian density describing the Rydberg–Rydberg interaction. Under the electric-dipole and rotating-wave approximations, $\hat{\mathcal{H}}_0$ and $\hat{\mathcal{H}}_1$ have the forms

$$\hat{\mathcal{H}}_0 = -\sum_{\alpha=2}^{3} \hbar \Delta_\alpha \hat{S}_{\alpha\alpha}(\mathbf{r}, t) - \hbar \left[\Omega_p \hat{S}_{12} + \Omega_c \hat{S}_{23} + \text{h.c.}\right] \tag{2}$$

$$\hat{\mathcal{H}}_1 = \mathcal{N}_a \int d^3 r' \hat{S}_{33}(\mathbf{r}', t) \hbar V(\mathbf{r}' - \mathbf{r}) \hat{S}_{33}(\mathbf{r}, t) \tag{2}$$

Here $\Delta_2 = \omega_p - (E_2 - E_1)/\hbar$ and $\Delta_3 = \omega_p + \omega_c - (E_3 - E_1)/\hbar$ are, respectively, the one- and two-photon detunings, with E_α being the eigenvalue of the energy of the state $|\alpha\rangle$; $\hat{S}_{\alpha\beta} \equiv \hat{\sigma}_{\beta\alpha} \exp\{i[(\mathbf{k}_\beta - \mathbf{k}_\alpha)\cdot\mathbf{r} - (\omega_\beta - \omega_\alpha + \Delta_\beta - \Delta_\alpha)t]\}$ is the atomic transition operator[124]; $\Omega_p = (\mathbf{e}_p \cdot \mathbf{p}_{12})\mathcal{E}_p/(2\hbar)$ and $\Omega_c = (\mathbf{e}_c \cdot \mathbf{p}_{23})\mathcal{E}_c/(2\hbar)$ are, respectively, half Rabi frequencies of the probe and control fields, with $\mathbf{p}_{\alpha\beta}$ the electric-dipole matrix elements associated with the transition $|\beta\rangle \leftrightarrow |\alpha\rangle$. The potential V in the expression of $\hat{\mathcal{H}}_1$ is taken as per Equation (1).[117,118,120,121]

The atomic dynamics is governed by the Heisenberg equation of motion for the operators $\hat{S}_{\alpha\beta}(\mathbf{r}, t)$, that is, $i\hbar\frac{\partial}{\partial t}\hat{S}_{\alpha\beta}(\mathbf{r}, t) = [\hat{H}, \hat{S}_{\alpha\beta}(\mathbf{r}, t)]$. Taking expectation values on the both sides of this equation, we obtain the optical Bloch equation involving one- and two-body reduced density matrices, with the form

$$\frac{\partial\hat{\rho}}{\partial t} = -\frac{i}{\hbar}\left[\hat{H}_0, \hat{\rho}\right] - \Gamma\left[\hat{\rho}\right] + \hat{R}[\hat{\rho}_{2\text{body}}] \tag{3}$$

where $\hat{\rho}(\mathbf{r}, t)$ is reduced one-body density matrix (DM) with matrix elements $\rho_{\alpha\beta}(\mathbf{r}, t) \equiv \langle\hat{S}_{\alpha\beta}(\mathbf{r}, t)\rangle$, Γ is a 3×3 relaxation matrix describing the spontaneous emission and dephasing. Due to the existence of the Rydberg–Rydberg interaction, two-body reduced DM, that is, $\hat{\rho}_{2\text{body}}(\mathbf{r}', \mathbf{r}, \mathbf{t})$ (with DM elements $\rho_{\alpha\beta,\mu\nu}(\mathbf{r}', \mathbf{r}, t)$), is involved in Equation (3), represented by the last term $\hat{R}[\hat{\rho}_{2\text{body}}]$. The explicit form of Equation (3) is given in Section S1, Supporting Information.

From Equation (3), we see that to get the solution of one-body DM elements $\rho_{\alpha\beta}$, equations for two-body elements $\rho_{\alpha\beta,\mu\nu}$ are needed, which, in turn, involve three-body DM element $\rho_{\alpha\beta,\mu\nu,\gamma\delta}$, and so on. As a result, one obtains a hierarchy of infinite equations for N-body DM elements ($N = 1, 2, 3, \cdots$) that must be solved simultaneously. To solve such a chain of equations, a suitable treatment beyond mean-field approximation must be adopted. A powerful one is the reduced density-matrix expansion, by which the hierarchy of the infinite equations is truncated consistently and the problem is reduced to solving a closed system of equations for the one- and two-body DM elements, as elaborated recently.[113,122,125]

The propagation of the probe field is governed by the Maxwell equation, which, under the slowly-varying-envelope approximation, is reduced to[122]

$$i\left(\frac{\partial}{\partial z} + \frac{1}{c}\frac{\partial}{\partial t}\right)\Omega_p + \frac{c}{2\omega_p}\nabla_\perp^2\Omega_p + \kappa_{12}\,\rho_{21} = 0 \tag{4}$$

Here $\nabla_\perp^2 = \partial_x^2 + \partial_y^2$ and $\kappa_{12} = \mathcal{N}_a\omega_p|\mathbf{p}_{12}|^2/(2\varepsilon_0 c\hbar)$

2.2. The Nonlinear Envelope Equation

Since the probe field is much weaker than the control field, the depletion of the atomic population in the ground state is small and a standard perturbation method can be applied to solve the system of Maxwell–Bloch (MB) equations (Equations (3) and (4)). To include the many-body correlations produced by the strong Rydberg–Rydberg interactions in a reasonable way, a beyond mean-field approximation[113,122,125] mentioned above must be used. Then, in the leading-order approximation, we obtain the solution for the probe field $\Omega_p = F(x, y, z, t)e^{iK(\omega)z - i\omega t}$, where F denotes a slowly varying envelope function and $K(\omega)$ stands for the linear dispersion relation, $K(\omega) = \omega/c + \kappa_{12}(\omega + d_{31})/[|\Omega_c|^2 - (\omega + d_{21})(\omega + d_{31})]$.

At the third-order approximation (details are given in Section S2, Supporting Information), we obtain the nonlinear equation for the probe-field envelope

$$i\frac{\partial}{\partial z}\Omega_p + \frac{c}{2\omega_p}\nabla_\perp^2\Omega_p - \frac{K_2}{2}\frac{\partial^2}{\partial T^2}\Omega_p + W\left|\Omega_p\right|^2\Omega_p + \Omega_p \int\int dxdy G(x' - x, y' - y)\left|\Omega_p(x', y', z, T)\right|^2 = 0 \tag{5}$$

where $T = t - z/V_g$, with $V_g = (\partial K/\partial\omega)^{-1}$ being the group velocity of the envelope, and $K_2 = \partial^2 K/\partial\omega^2$ defines the group-velocity dispersion. The last two terms in Equation (5) contributed, respectively, from the local and nonlocal optical Kerr nonlinearities in the system. Explicit expressions of the coefficients W and G (nonlocal nonlinear response function) are given in Section S2, Supporting Information. The local optical Kerr nonlinearity is contributed to by the short-range interaction between photons and atoms, proportional to the atomic density $\mathcal{N}_a$, whereas the nonlocal optical Kerr nonlinearity is contributed by the long-range Rydberg–Rydberg interaction, which scaled quadratically with the atomic density (i.e., proportional to $\mathcal{N}_a^2$).

Equation (5) can be further written into the non-dimensional form

$$i\frac{\partial u}{\partial\zeta} + \left(\frac{\partial^2}{\partial\xi^2} + \frac{\partial^2}{\partial\eta^2}\right)u + d\frac{\partial^2 u}{\partial\tau^2} + w|u|^2u + u \int\int d\xi' d\eta' g(\xi' - \xi, \eta' - \eta)\left|u\left(\xi', \eta', \zeta, \tau\right)\right|^2 = 0 \tag{6}$$

where $u = \Omega_p/U_0$, $\zeta = z/(2L_{\text{diff}})$, $(\xi, \eta) = (x, y)/R_0$, $\tau = T/\tau_0$, $d = -\text{sgn}(K_2)L_{\text{diff}}/L_{\text{disp}}$, $w = 2L_{\text{diff}}|U_0|^2W$, and $g = 2L_{\text{diff}}R_0^2|U_0|^2G(\xi' - \xi, \eta' - \eta)$, with the diffraction and dispersion lengths respectively given by $L_{\text{diff}} = \omega_p R_0^2/c$ and $L_{\text{disp}} = \tau_0^2/|K_2|$. Here U_0, R_0, and τ_0 are typical half Rabi frequency, beam radius in the transverse plane (x, y), and temporal duration of the probe-field envelope, respectively.

To address a typical example, we consider laser-cooled strontium ^{88}Sr atoms, with atomic levels $|1\rangle = |5s^2\ ^1S_0\rangle$, $|2\rangle = |5s5p\ ^1P_1\rangle$, and $|3\rangle = |5sns\ ^1S_0\rangle$. For the principal quantum number $n = 60$, the dispersion parameter $C_6 \approx 2\pi \times 81.6\,\text{GHz}\,\mu\text{m}^6$ (which implies the Rydberg–Rydberg interaction is attractive). The spontaneous emission decay rates are $\Gamma_{12} \approx 2\pi \times 32$ MHz and $\Gamma_{23} \approx 2\pi \times 16.7$ kHz, while the detunings are taken to be $\Delta_2 = -2\pi \times 240$ MHz and $\Delta_3 = -2\pi \times 0.16$ MHz. The density of the atomic gas is $\mathcal{N}_a = 9 \times 10^{10}$ cm^{-3}, and the half Rabi frequency of the control field is $\Omega_c = 2\pi \times 5$ MHz. Since $\Delta_2 \gg \Gamma_{12}, \Delta_3$, which makes the system works in a dispersive nonlinearity regime, the imaginary parts of coefficients in Equation (5) are much smaller than the corresponding real parts, and hence Equation (6) can be approximately considered as a real-coefficient one.

The nonlocal nonlinear response function $g(\xi' - \xi, \eta' - \eta)$ has a very complicated expression. For the convenience of the sub-

sequent variational calculation for the interaction force between solitons, we approximate it by a Gaussian function, that is,

$$g \approx g_{\rm F} \equiv \frac{g_0}{\left(0.64\,\sigma\sqrt{\pi}\right)^2} e^{-\frac{(\xi-\xi')^2+(\eta-\eta')^2}{(0.64\,\sigma)^2}} \tag{7}$$

(details of relations between g and $g_{\rm F}$ are given in Section S3, Supporting Information), where $g_0 = \int\int d\xi d\eta g(\xi'-\xi, \eta-\eta)$ is a constant and σ characterizes the nonlocality degree of the nonlinearity, defined as

$$\sigma = R_{\rm b}/R_0 \tag{8}$$

Here $R_{\rm b} = (|C_6/\delta_{\rm EIT}|)^{1/6}$ denotes the Rydberg blockade radius, where $\delta_{\rm EIT} \approx |\Omega_{\rm c}|^2/|\Delta_2|$ is the linewidth of the EIT transmission spectrum for $|\Delta_2| \gg \Gamma_{12}$.[120,121] With the values of parameters adopted above, we get $R_{\rm b} \approx 9.6\,\mu$m. If $R_{\rm b} \ll R_0$ (i.e., $\sigma \to 0$, the local limit), the nonlocal response reduces to the delta function, that is, $g_0\delta(\xi-\xi', \eta-\eta')$. In this limit, the nonlocal Kerr nonlinearity is reduced to the usual local term, $g_0|u|^2u$. If $R_{\rm b} \gg R_0$ ($\sigma \to \infty$, the strongly nonlocal limit), the nonlocal response, given by Equation (7), reduces to a linear term $g_0 Pu$, where $P = \int\int d\xi d\eta\,|u|^2$ is the power of the probe field (this limit corresponds to the so-called "accessible-soliton" model, which is actually a limit one[98,100]).

The susceptibility of the probe field is defined by $\chi_{\rm p} = \mathcal{N}_{\rm a}(\mathbf{e}_{\rm p}\cdot\mathbf{p}_{12})^2\rho_{21}/(\varepsilon_0\hbar\Omega_{\rm p})$, which can be further expressed as $\chi_{\rm p} \approx \chi^{(1)} + \chi^{(3)}_{\rm loc}|\mathcal{E}_{\rm p}|^2 + \chi^{(3)}_{\rm nloc}|\mathcal{E}_{\rm p}|^2$. In this expansion, $\chi^{(1)}$ represents the linear susceptibility; $\chi^{(3)}_{\rm loc}$ and $\chi^{(3)}_{\rm nloc}$ are respectively the local and nonlocal third-order nonlinear susceptibilities, associated to the coefficients of Equation (5) as

$$\chi^{(3)}_{\rm loc} = \frac{2(\mathbf{e}_{\rm p}\cdot\mathbf{p}_{12})^2}{k_{\rm p}\hbar^2}W, \quad \chi^{(3)}_{\rm nloc} = \frac{2(\mathbf{e}_{p}\cdot\mathbf{p}_{12})^2}{k_{\rm p}\hbar^2}\int\int dx'dy'G(x'-x, y'-y) \tag{9}$$

With the system's parameters introduced above, we obtain $\chi^{(3)}_{\rm loc} \approx 10^{-11}$ m^2 V^{-2} and $\chi^{(3)}_{\rm nloc} \approx 10^{-8}$ m^2 V^{-2}, that is, the nonlocal optical Kerr nonlinearity is three orders of magnitude stronger than the local one due to the Rydberg–Rydberg interaction.

3. Nonlocal (2+1)D Spatial Solitons and Vortex Molecules

3.1. The Interaction between Two Nonlocal (2+1)D Spatial Solitons

We now address the interaction force between two nonlocal (2+1)D[126] spatial solitons. By setting $d = 0$ (which implies that time duration τ_0 of the probe field is large enough to make the dispersion of the system negligible, valid for $L_{\rm disp} \gg L_{\rm diff}$), Equation (6) reduces to the form

$$i\frac{\partial u}{\partial\zeta} + \left(\frac{\partial^2}{\partial\xi^2} + \frac{\partial^2}{\partial\eta^2}\right)u + w|u|^2u + u \int\int d\xi'd\eta' g(\xi'-\xi, \eta'-\eta)\left|u\left(\xi', \eta', \zeta\right)\right|^2 = 0 \tag{10}$$

The Lagrangian corresponding to this equation is $L = \int\int_{-\infty}^{\infty} d\xi d\eta\,\mathcal{L}$, with the density $\mathcal{L} = \frac{i}{2}(uu^*_\zeta - u^*u_\zeta) + |u_\xi|^2 + |u_\eta|^2 - \frac{w}{2}|u|^4 - \frac{1}{2}|u|^2\int\int g(\xi-\xi', \eta-\eta')|u(\xi', \eta', \zeta)|^2 d\xi d\eta$.

The bound state of two solitons (i.e., the two-soliton "molecule") is sought by means of the ansatz

$$u(\xi, \eta) = u_+(\xi, \eta) - u_-(\xi, \eta) \tag{11}$$

with each soliton approximated by a Gaussian, that is,

$$u_\pm = A\,e^{-[(\xi\pm D/2)^2+\eta^2]/(2a^2)+ib(\xi^2+\eta^2)+i\phi} \tag{12}$$

It includes two identical Gaussian beams, located at different positions $(-D/2, 0)$ and $(D/2, 0)$, with a π phase difference. Variational z-dependent parameters are A (amplitude), D (spatial separation), b (chirp), and ϕ (phase), while the total power $P = 2\pi a^2A^2[1 - e^{-D^2/(4a^2)}]$ is a conserved quantity. Due to the π phase difference, there is a repulsive interaction between the two solitons. Such a repulsive interaction is expected to balance the attractive interaction induced by the self-focusing nonlocal optical Kerr nonlinearity (induced by the attractive Rydberg–Rydberg interactions), and thus help to form a stable two-soliton molecule.[127]

Following the standard procedure of the variational approximation,[113,127–129] one can derive evolution equations for the variational parameters A, D, b, and ϕ, and hence the equation of motion for the spatial separation D between center-of-mass positions of the interacting solitons

$$\frac{dD}{d\zeta} = \frac{16b\left[1 - e^{-D^2/(4a^2)}\right]\left[(a^2 + D^2/4)e^{D^2/(4a^2)} - a^2\right]}{D[(e^{D^2/(4a^2)} - 1) - D^2/(4a^2)]} \tag{13}$$

This equation can be cast in the form of the equation of motion for the Newtonian particle $M_{\rm s}(d^2D/d\zeta^2) = -\partial U/\partial D$, where $M_{\rm s}$ is the effective mass of each soliton and $U = U(D)$ denotes the effective potential which accounts for the interaction between the two solitons.

We recall that in locally nonlinear media, the interaction between two solitons is determined by the overlap between their wave functions, which quickly decays as the separation between them increases. Normally, the interaction becomes negligible if the separation between the solitons is 2–3 times greater than their widths.[114] Nevertheless, for nonlocally nonlinear media the interaction between two solitons takes place when they have no tangible overlap, which may be called *contactless* interaction. To demonstrate this clearly, we introduce an overlap parameter

$$J = \frac{\int\int_{-\infty}^{\infty} d\xi d\eta |u_+u_-|^2}{\int\int_{-\infty}^{\infty} d\xi d\eta |u_+|^2 \int\int_{-\infty}^{\infty} d\xi d\eta |u_-|^2} \tag{14}$$

where u_+ and u_- are introduced in Equation (12). **Figure 2**a shows J as a function of σ for the ansatz (11), with system's parameters $A = 2$, $b = 0$, $a = 1$, and $\phi = 0$. We see that J is non-vanishing only for $\sigma \leqslant 0.2$.

For locally nonlinear media (for which $\sigma \approx 0$), the interaction between two solitons is negligible when there is no overlap between the solitons. However, the interaction between the two solitons is non-zero even they has no overlap if the nonlocality degree

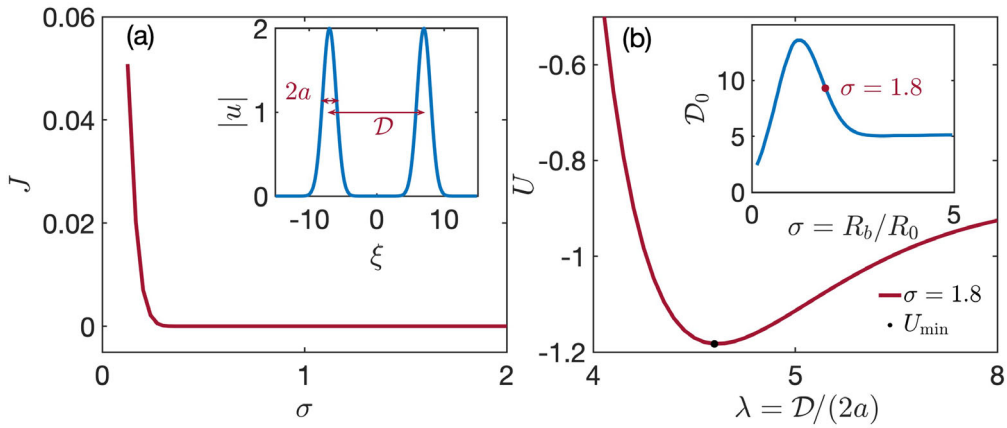

Figure 2. Contactless interaction between two-soliton molecule. a) The overlap measure J, defined as per Equation (14), as a function of the nonlocality degree σ of the Kerr nonlinearity. Inset: Amplitude $|u|$ of the two-soliton set as a function of ξ. Inset: $|u|$ for $\eta \equiv \gamma/R_0 = 0$. b) The effective potential U of the soliton–soliton interaction versus $\lambda = \mathcal{D}/(2a)$ with $\sigma = 1.8$. The black dot marks the minimum of the potential energy, $U_{\min}$. Inset: The equilibrium separation between the solitons, $\mathcal{D}_0$, versus the nonlocality degree σ.

of the Kerr nonlinearity reaches to a critical value (i.e., $\sigma \geq 0.2$ in the present Rydberg gas). To characterize the size of the SM, we define the separation-width ratio

$$\lambda = \mathcal{D}/(2a), \tag{15}$$

that is, the ratio of the separation of the two solitons, $\mathcal{D}$, to the width of a single soliton, $2a$ (see Figure 2a). Shown in Figure 2b is the effective interaction potential U (calculated following ref. [127]) as a function of λ for the ansatz (11) with $\sigma = 1.8$, $A = 2$, $b = 0$, $a = 1$, and $\phi = 0$. It is seen that U has a minimum $U_{\min}$ at $\lambda \approx 4.6$, which corresponds to separation $\mathcal{D} = \mathcal{D}_0 \approx 9.2$ between the two solitons. Thus, it is possible to expect the existence of the SM with size close to $\mathcal{D}_0$. Because the width of each soliton in the SM is $2a = 2$, and the separation between them at the equilibrium position is $\mathcal{D}_0 = 9.2$, the effective soliton interaction is indeed *contactless*. The reason for the occurrence of such a contactless interaction between the solitons is due to the giant nonlocal Kerr nonlinearity, which induces significant interaction between the solitons while their wave functions exhibit no overlap in space. On the other hand, in media with the local Kerr optical nonlinearity, the interaction between solitons, and hence the formation of SMs, is determined by the overlap of "tails" of the wave functions of adjacent solitons, and becomes negligible when there is no overlap between the solitons. Consequently, SMs in locally nonlinear media usually have only a small separation-width ratio.

Shown in the inset to Figure 2b is the equilibrium separation $\mathcal{D}_0$ between the two solitons as a function of the degree of the nonlocality of the Kerr nonlinearity σ. It is seen that, as σ increases, $\mathcal{D}_0$ grows at first, reaches its maximum, and decreases, eventually saturating to a small value. Thus, by changing σ, one can control $\mathcal{D}_0$ and thus the size of the SM. The maximum value of $\mathcal{D}_0$ is obtained at $\sigma \approx 1.6$, which is about 13.6, and the corresponding size of the SM in physical units is $13.6\, R_0 \approx 82$ μm. Such a value is a realistic one for the experimental observation in Rydberg gases.[130]

3.2. The Formation and Propagation of Nonlocal (2+1)D Spatial Soliton Molecules

3.2.1. Two-Soliton Molecules

We proceed to the investigation of the formation and propagation of stable (2+1)D spatial SMs by means of numerical simulations of Equation (6). **Figure 3**a shows the amplitude of a typical two-soliton molecule at $\zeta = 0$ and 12, the latter value corresponding, in physical units, to $z \approx 1.2$ cm for $L_{\text{diff}} \approx 0.49$ mm. The initial condition for the simulation are chosen as per ansatz (11) with a small random perturbation introduced by the factor

$$\text{Random} = 1 + \varepsilon R(\xi, \eta) \tag{16}$$

multiplying the initial configuration. Here, $\varepsilon \ll 1$ is the amplitude of the perturbation, and R is a random variable uniformly distributed in the interval [0,1]. Parameters of the initial condition are taken as $\sigma = 1.8$, $A = 2$, $a = 1$, $\mathcal{D} = \mathcal{D}_0 = 9.2$ ($\lambda \approx 4.6$), $b = \phi = 0$, and $\varepsilon = 0.05$. The SM is found to be stable as it relaxes to the self-cleaned form close to the unperturbed one and undergoes no apparent distortion during propagation.

Shown in Figure 3b is the case where the two solitons are initially placed in their equilibrium positions. We see that the SM is stable and without conspicuous intrinsic oscillations. However, when the two solitons are slightly shifted from their equilibrium positions (by taking $\mathcal{D} = 12 > \mathcal{D}_0 = 9.2$ at $\zeta = 0$), they perform a small oscillation around the equilibria, if no additional perturbations are introduced; see Figure 3c. The existence of such an *excited state* of the SM clearly corroborates that the static copropagation of the two solitons in Figure 3a (as well as in Figures 3e, 5a, and 6 below) is indeed provided by the fact that they form the stable bound state, rather than by trivial absence of interaction between two well-separated solitons.

Figure 3d illustrates the same outcome of the evolution, except that we have added initial velocities $v = \pm 0.5$ to the solitons, to admit the consideration of the generation of the two-soliton molecule under experimentally relevant conditions, and

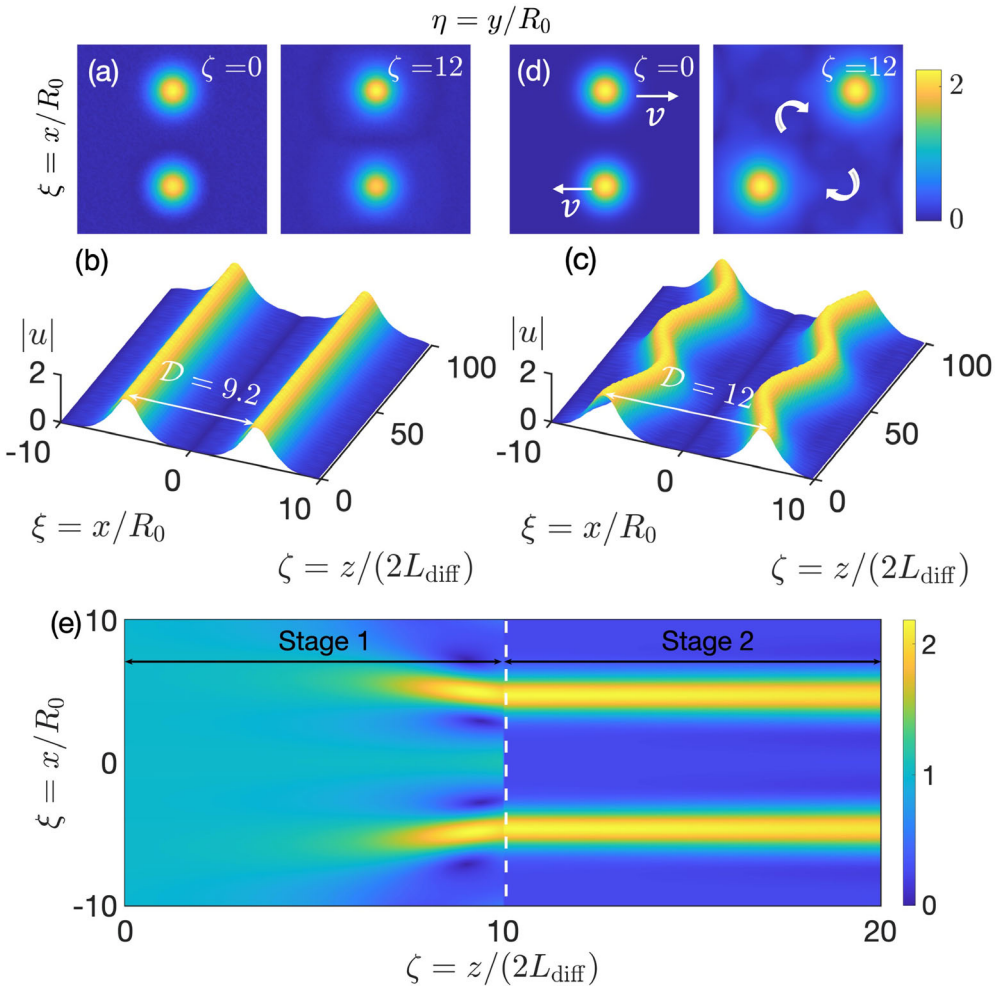

Figure 3. The propagation of a (2+1)D spatial two-soliton molecule. a) Amplitude profiles $|u|$, at different propagation distances, $\zeta = z/(2L_{\rm diff}) = 0$ and 12. When two solitons are placed in their equilibrium positions, they form a stable molecule. Here $\sigma = 1.8$, $A = 2$, $a = 1$, $b = 0$, $\phi = 0$, and $D = D_0 = 9.2$. b) When the solitons are placed in their equilibrium positions, they form a stable (2+1)D spatial SM. Parameters are the same as in (a). c) When the solitons are initially shifted from their equilibrium positions, they perform a small oscillation around the equilibria, if no additional perturbations are introduced. Parameters are the same as (a). d) Amplitude profiles $|u|$ with nonzero initial velocity $v = \pm 0.5$ at propagation distances $\zeta = z/(2L_{\rm diff}) = 0$ and 12. In that case, white arrows designate the direction of the rotation of the emerging SM. e) The buildup of stable (2+1)D spatial SMs. It display the first ($0 \leqslant \zeta \leqslant 10$) and second stages ($10 \leqslant \zeta \leqslant 20$) of the evolution. Shown in (b,c,e) are for $|u|$ in the cross section $\eta \equiv y/R_0 = 0$.

the study of the role of the incident velocity of the solitons, see ref. [131]). In this case, the SM exhibits persistent rotation, keeping its stability in the course of the propagation. As the rotation results in an additional centrifugal force acting on each soliton, the size of the rotating SM is larger than that of the non-rotating one.

Another way for spontaneous generation of (2+1)D spatial SMs is provided by the modulational instability (MI). Figure 3e shows the MI-driven buildup of stable (2+1)D SMs. The initial condition for the simulations is chosen as a slightly perturbed plane-wave state, that is, $1 + \varepsilon \cos(0.5\xi)$ with $\varepsilon = 10^{-4}$. It is seen that, at the first stage of the evolution, $0 \leqslant \zeta \leqslant 10$, the MI develops and two bright solitons appears, which bind into a soliton molecule along with some small radiations. At the second stage, $10 \leqslant \zeta \leqslant 20$, we propagate the emerging SM after filtering out small radiation. It is found that the SM, built at the first stage of the evolution, remains stable over a very long distance.

The input power used for the generation of (2+1)D spatial SMs considered here can be estimated by computing the corresponding Poynting's vector integrated over the cross-sectional area of the probe beam, that is, $P = \int dS(\mathbf{E}_{\rm p} \times \mathbf{H}_{\rm p}) \cdot \mathbf{e}_z$, where $\mathbf{e}_z$ is the unit vector in the propagation direction. Assuming that $\mathbf{E}_{\rm p} = (E_{\rm p}, 0, 0)$ and $\mathbf{H}_{\rm p} = (0, H_{\rm p}, 0)$, with $H_{\rm p} = \varepsilon_0 c n_{\rm p} E_{\rm p}$ ($n_{\rm p}$ is the refractive index), one can readily obtain

$$P_{\rm gen} = 2\varepsilon_0 c n_{\rm p} S_0 \left(\frac{2\hbar}{p_{13}}\right)^2 |\Omega_{\rm p}|^2 \approx 3.6\,\mu{\rm W} \tag{17}$$

where S_0 denotes the cross-sectional area of the probe beam.

Thus, very low input power is sufficient for the creation of such nonlocal (2+1)D spatial two-soliton molecules with the help of the giant nonlocal Kerr nonlinearity in the present system. This fact may be highly beneficial for applications to optical data procession and transmission, using low-level light powers.

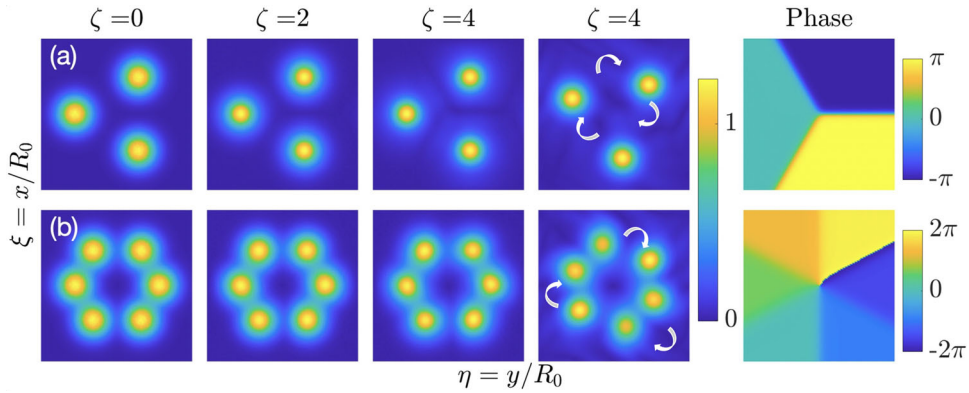

Figure 4. The simulated propagation of a (2+1)D necklace-shaped SM built of N solitons with $N = 3$ and 6. a) The amplitude profile of $|u(\xi, \eta)|$ with $(N, m) = (3, 1)$ in the plane of $\xi = x/R_0$ and $\eta = y/R_0$ at different propagation distances $\zeta = z/(2L_{\text{diff}}) = 0$, 2, 4, respectively. The fourth column are amplitude profiles $|u|$ with nonzero initial tangential velocity $v = 0.6$ at propagation distances $\zeta = z/(2L_{\text{diff}}) = 4$. In that case, white arrows designate the direction of the rotation of the emerging SM. The rightmost panel shows the phase distribution in the (2+1)D spatial SM at $\zeta = 0$. The parameters are $A = 1.2$, $\rho_0 = 5$, $a = 1.45$, and $b = 0$. b) The same as in (a), but for $(N, m) = (6, 2)$.

3.2.2. Multi-Soliton Molecules

Besides the two-soliton SMs, the Rydberg-EIT system can also support stable nonlocal (2+1)D N-soliton molecules with $N \geq 3$. The N-soliton molecule in a ring-shape configuration (i.e., as a *soliton necklace*, which may be readily supported by nonlocal nonlinearities[132]) can be sought by using the trial solution

$$u = A \sum_{n=1}^{N} e^{-[(\xi-\xi_n)^2+(\eta-\eta_n)^2]/(2a^2)+ib(\xi^2+\eta^2)+i(\phi_n+\phi)} \tag{18}$$

where $(\xi_n, \eta_n) = \rho_0[\cos(2\pi n/N), \sin(2\pi n/N)]$ is the center-of-mass position of the nth Gaussian beam, with ρ_0 being the ring's radius. The phase of the nth beam is $\phi_n = 2\pi mn/N$; the overall phase imposed on the ring-shaped configuration is $2\pi m$. Here m is a positive integer taking in the interval $(N/4, N/2]$. In this way, the phase difference between two adjacent beams, $\phi_{n+1} - \phi_n$, is given by $\pi/2 < \phi_{n+1} - \phi_n \leqslant \pi$, which introduces a repulsive interaction between the beams and balances the attractive interaction due to the self-focusing nonlocal Kerr nonlinearity, and hence is in favor of the formation of a N-soliton molecule. The meanings of parameters A, a, b, and ϕ in ansatz (18) is the same as in Equation (12). Following the variational procedure similar to that used above, one can derive equations for parameters A, ρ_0, b, and ϕ. As the number of the variational parameters for N-soliton molecules is much larger than for the two-soliton ones, we resort to numerical methods for solving the variational equations.

Figure 4a,b displays, respectively, the simulated propagation of three- and six-soliton molecules. The initial conditions are chosen as per Equation (18), respectively with $(N, m) = (3, 1)$ and $(N, m) = (6, 2)$, multiplied by the random-perturbation factor (Equation (16)). The parameters of the input are taken as $A = 1.2$, $\rho_0 = 5$, $a = 1.45$, $b = \phi = 0$, and $\varepsilon = 0.05$. We find that both 3- and 6-soliton molecules are stable, relaxing to self-cleaned forms close to the unperturbed ones. The fourth column shows the same outcome of the evolution, except that we have added initial tangential velocities $v = 0.6$ to the solitons, hence the SM exhibits persistent rotation, keeping its stability in the course of the propagation. The rightmost panel shows the initial phase distribution in the (2+1)D spatial SM.

3.3. Nonlocal (2+1)D Vortex Molecules

Stable (2+1)D spatial SMs may also be composed of vortex solitons. As an example, we consider a bound state of two vortex solitons built as per ansatz (11), with each component $u_{\pm}$ taken as the Laguerre–Gaussian beam

$$u_{\pm} = A\left(\frac{\sqrt{2}r_{\pm}}{a}\right)^{|l|} e^{-r_{\pm}^2/a^2} L_{\text{p}}^{|l|}\left(\frac{2r_{\pm}^2}{a^2}\right) e^{il\varphi} \tag{19}$$

Here A and a are the soliton's amplitude and radius, $r_{\pm} = \sqrt{(\xi \pm \mathcal{D}/2)^2 + \eta^2}$, $L_{\text{p}}^{|l|}$ is the generalized Laguerre–Gaussian polynomial, with the azimuthal (radial) index l (p), and φ is the azimuthal angle. The ansatz based on Equations (11) and (19) introduces the superposition of two Laguerre–Gaussian beams with identical shapes, opposite signs, and centers placed at points $(\pm\mathcal{D}/2, 0)$.

Figure 5a (see also Figure 1b) shows the propagation of a typical (2+1)D two-vortex molecule. Here, we fix $l = 1$ and $p = 0$ in the Laguerre–Gaussian polynomial in Equation (19). The input, composed as per Equations (11) and (19), includes the perturbation factor in Equation (16) too. Parameters of the input are $A = 3.9$, $a = 1.45$, $\mathcal{D} = 10$, and $\varepsilon = 0.05$. The two-vortex molecule has a large size, with the equilibrium separation between pivots of the two vortices $\mathcal{D}_0 = 10$, corresponding to 60 μm in physical units (in experiments with BEC, "large" is usually a size which is essentially larger than 10 μm[133]). Such a contactless interaction between the two vortices and the formation of the vortex molecule is also due to the nonlocal Kerr nonlinearity contributed by the long-range Rydberg–Rydberg interaction between the atoms.

We have also simulated the propagation of a three-vortex molecule, as shown in Figure 5b. As well as its two-vortex counterpart, it is found to be stable. The fourth column of Figure 5a,b shows the same outcome of the evolution, except that we have

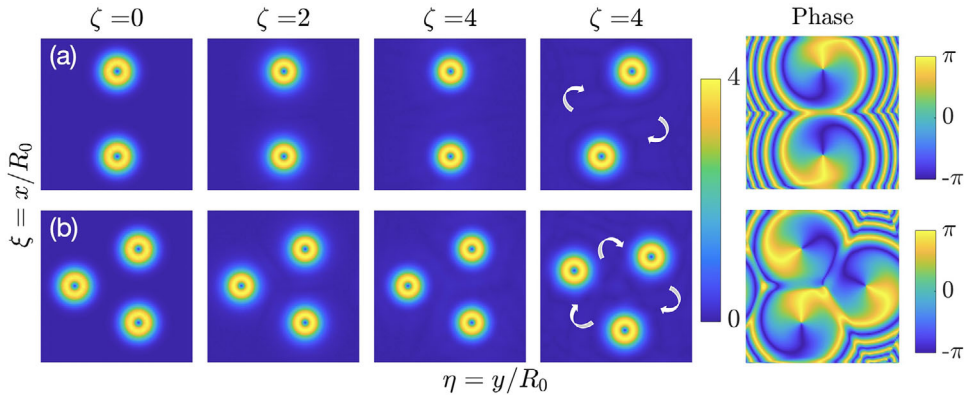

Figure 5. The propagation of a (2+1)D vortex molecule with built of a two (a) or three (b) vortices. a) The amplitude profile of $|u(\xi,\eta)|$ for the two-vortex SM in the plane of ($\xi = x/R_0$, $\eta = y/R_0$) at different propagation distances $\zeta = z/(2L_{\text{diff}}) = 0,\ 2,\ 4$. The fourth column are amplitude profiles $|u|$ with nonzero initial tangential velocity $v = 0.6$ at propagation distances $\zeta = z/(2L_{\text{diff}}) = 4$. In that case, white arrows designate the direction of the rotation of the emerging SM. The rightmost panel shows the phase distribution in the (2+1)D spatial SM at $\zeta = 2$. The azimuthal and the radial indices are $l = 1$ and $p = 0$ for the Laguerre–Gaussian polynomial, see Equation (19). Other parameters are $A = 3.9$, $a = 1.45$, and $\mathcal{D} = 10$. b) The same as in (a), but for $N = 3$.

added initial tangential velocities $v = 0.6$ to the vortex, hence the vortex molecule exhibits persistent rotation, keeping its stability in the course of the propagation. The rightmost panel shows the phase distribution in the (2+1)D spatial vortex molecules at $\zeta = 2$.

4. Nonlocal (3+1)D Soliton and Vortex Molecules, Their Storage and Retrieval

4.1. Nonlocal (3+1)D Soliton and Vortex Molecules

The realization of (3+1)D[134] spatiotemporal solitons is a long-standing challenging goal of optical physics.[82,87,88] As mentioned above (3+1)D spatiotemporal solitons are strongly unstable in conventional optical media with the local Kerr nonlinearity. In a recent work, it has been shown that stable (3+1)D spatiotemporal solitons may exist in a cold Rydberg atomic gas, being supported by a two-step self-trapping mechanism.[113]

To proceed, we first demonstrate that stable (3+1)D spatiotemporal soliton/vortex molecules are available in the Rydberg atomic gas. To form such states, dispersion of the probe field is necessary, which can be secured by using a probe pulse with a short time duration. To this end, we adopt a new set of system's parameters: $\mathcal{N}_a = 10^{11}$ cm^{-3}, $\Delta_2 = -2\pi \times 240$ MHz, $\Delta_3 = -2\pi \times 0.03$ MHz, $\Omega_c = 2\pi \times 8$ MHz, and $\tau_0 = 0.1\,\mu$s. With these parameters, the scaled coefficients in Equation (6) are $d \approx 0.19$ and $w \approx 0.25$. The (3+1)D spatiotemporal two-soliton molecules can be sought by using ansatz (12) for a single soliton, multiplying it by the temporal-localization factor, $\text{sech}(\tau/a_\tau)\exp(ib_\tau\tau^2)$, where a_τ and b_τ stand for the temporal width and chirp of the probe pulse.

Shown in **Figure 6**a is the propagation of a typical (3+1)D spatiotemporal two-soliton molecule. The initial condition used in the numerical simulation again includes the small random perturbation. Parameters of the input are $A = 1.6$, $\mathcal{D} = 8$, $a = 1.2$, $a_\tau = 1$, $b = b_\tau = \phi = 0$, and $\varepsilon = 0.05$. The (3+1)D spatiotemporal SM is found to be stable in the course of the propagation.

With the parameters given above, the propagation velocity of the (3+1)D spatiotemporal SM, produced by the formula $V_g = (\partial K/\partial\omega)^{-1}$ at $\omega = 0$, is

$$V_g = \left\{ \frac{1}{c} + \kappa_{12} \frac{|\Omega_c|^2 + (\omega + d_{31})^2}{[|\Omega_c|^2 - (\omega + d_{21})(\omega + d_{31})]^2} \right\}^{-1} \approx 3.4 \times 10^{-5}\, c, \tag{20}$$

and the required generation power is estimated to be $P_{\text{gen}} = 6.8\,\mu$W. Thus, the SM travels indeed with an ultraslow velocity (in comparison to c) and may be created by a very low power, which is due to the interplay of the EIT and giant nonlocal Kerr nonlinearity induced by the Rydberg–Rydberg interaction between the atoms.

We have also carried out a numerical simulation for the propagation of a nonlocal (3+1)D spatiotemporal two-vortex molecule, with individual vortex solitons taken as per ansatz (19) times $\text{sech}(\tau/a_\tau)\exp(ib_\tau\tau^2)$. Figure 6b shows the propagation of a typical two-vortex SM with small perturbations. The parameters used in the simulation are $A = 2.5$, $a = 1.3$, $a_\tau = 1$, $\mathcal{D} = 8$, $b = b_\tau = \phi = 0$, and $\varepsilon = 0.05$. The two-vortex SM is also found to be quite stable, as well as the zero-vorticity spatiotemporal SM.

4.2. Storage and Retrieval of Nonlocal (3+1)D Soliton and Vortex Molecules

Keeping memory of optical pulses in atomic gases (i.e., storage of incident pulses, with ability to retrieve them), provided by the EIT technique, has attracted much interest.[135–146] Here we demonstrate that the storage and retrieval of (3+1)D spatiotemporal soliton/vortex molecules are possible in the present Rydberg-EIT system. To this end, we investigate the evolution of the (3+1)D spatiotemporal molecules, considered above, by solving the MB

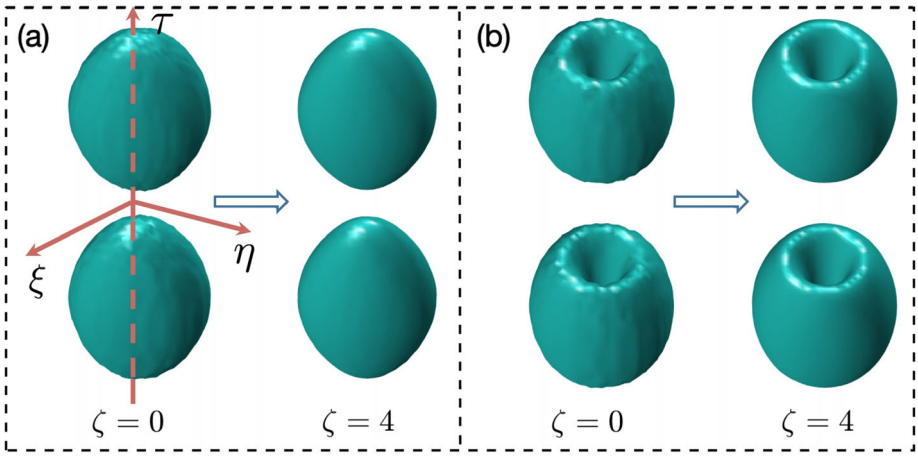

Figure 6. The simulated propagation of a (3+1)D spatial-temporal two-soliton molecule (a) and two-vortex molecule (b). a) Isosurfaces of $|u|$ of the (3+1)D two-soliton molecule at propagation distances $\zeta = z/(2L_{\text{diff}}) =$ 0 and 4, respectively. The parameters are $A = 1.6$, $a = 1.2$, $D = 8$, $a_\tau = 1$, and $b = b_\tau = 0$. b) The same as in (a), but for a (3+1)D spatial-temporal two-vortex molecule, with the azimuthal and the radial indices $l = 1$ and $p = 0$ in Equation (19). The parameters are $A = 2.5$, $a = 1.3$, $D = 8$, $a_\tau = 1$, and $b = b_\tau = 0$.

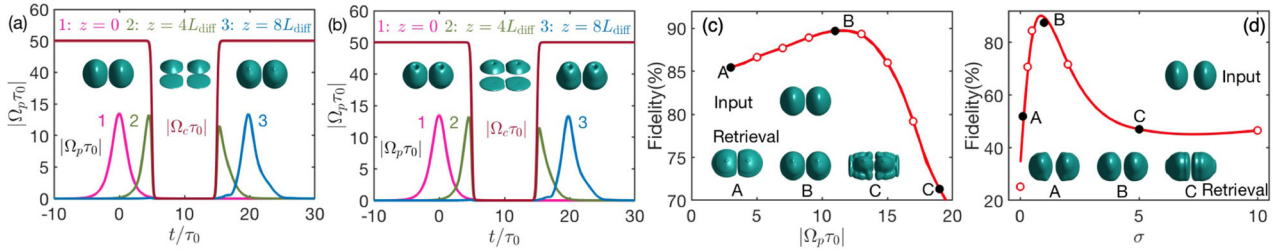

Figure 7. Storage and retrieval of (3+1)D two-soliton molecule and two-vortex molecule. a) The storage and retrieval of a nonlocal (3+1)D spatial-temporal two-soliton molecule. The red solid line shows switching the control field $|\Omega_c\tau_0|$ on and off. Curves 1, 2, and 3 are temporal profiles of the probe pulse $|\Omega_p\tau_0|$, respectively, at $z = 0$ (the initial condition), $z = 4L_{\text{diff}}$ (just before the storage), and $8L_{\text{diff}}$ (just after the retrieval), with $L_{\text{diff}} = 0.87$ mm; the corresponding isosurface plots for $|\Omega_p\tau_0| = 0.5$ are shown. b) The same as (a) but for the storage and retrieval a nonlocal (3+1)D spatial-temporal two-vortex molecule. c) The fidelity $\eta\mathcal{J}$ as a function of the probe-field amplitude $|\Omega_p\tau_0|$ at $\zeta = z/(2L_{\text{diff}}) = 4$. The isosurfaces of the input probe field (upper inset) and the retrieved ones at different $|\Omega_p\tau_0|$ (lower insets) are also illustrated. d) The fidelity $\eta\mathcal{J}$ as a function of the nonlocality degree σ at $\zeta = z/(2L_{\text{diff}}) = 4$. The isosurfaces of the input probe field (upper inset) and the retrieved ones at different σ (lower insets) are also illustrated.

Equations (3) and (4) numerically, using a time-dependent control field

$$\Omega_c(t) = \Omega_{c0}\left[1 - \frac{1}{2}\tanh\left(\frac{t - T_{\text{off}}}{T_s}\right) + \frac{1}{2}\tanh\left(\frac{t - T_{\text{on}}}{T_s}\right)\right] \quad (21)$$

which provides switching action for the probe field. Here T_{off} and T_{on} are, respectively, the times at which the control field is switched off and on. The switching duration is T_s and the storage time is $T_{\text{on}} - T_{\text{off}}$. Importantly, the switching speed of the control laser has a marginal effect on the quality of the SM storage and retrieval. This is because the (3+1)D spatiotemporal SM in the present system propagates with an ultraslow velocity, due to the EIT effect.[147]

Shown in **Figure 7**a is the evolution of the probe-pulse amplitude $|\Omega_p\tau_0|$ in the course of the storage and retrieval process. The shapes of the probe pulse at $z = 0$ (before storage), $z = 4L_{\text{diff}}$ (at the beginning of storage), and $z = 8L_{\text{diff}}$ (after the retrieval) are shown for $L_{\text{diff}} = 0.87$ mm. It is seen that switching off the control field provides for the storage of the (3+1)D spatiotemporal SM in the atomic medium, which is retrieved when the control field is switched on again. Further, the retrieved spatiotemporal SM has nearly the same shape as the original one prior to the storage. In the course of the storage, the information carried by the SM is converted into that kept in the atomic spin wave (i.e., the coherence matrix element ρ_{13}). A slight deformation affecting the optical memory is due to dissipation, including spontaneous emission and dephasing, as well as weak imbalance between diffraction, dispersion, and nonlinearity. We have also explored the storage and retrieval of (3+1)D spatiotemporal vortex molecules. Similar results are obtained for the vortex bound states, as shown in Figure 7b.

The quality of the storage and retrieval of nonlocal (3+1)D spatiotemporal SMs can be characterized by efficiency η and fidelity $\eta\mathcal{J}$, where η and $\mathcal{J}$ are defined as

$$\eta = \frac{\int_{T_{\text{on}}}^{\infty} dt \int\int dxdy|\Omega_p^{\text{out}}(x,y,t)|^2}{\int_{-\infty}^{T_{\text{off}}} dt \int\int dxdy|\Omega_p^{\text{in}}(x,y,t)|^2} \quad (22a)$$

$$\mathcal{J} = \frac{|\int_{-\infty}^{\infty} dt \int\int dxdy\Omega_p^{\text{out}}(x,y,t-\Delta T)\Omega_p^{\text{in}}(x,y,t)|^2}{\int_{-\infty}^{T_{\text{off}}} dt \int\int dxdy|\Omega_p^{\text{in}}|^2 \int_{T_{\text{on}}}^{\infty} dt \int\int dxdy|\Omega_p^{\text{out}}|^2} \quad (22b)$$

Based on the results obtained in Figure 7a,b, we obtain $\eta = 90.39\%$, $\mathcal{J} = 98.81\%$, and $\eta\mathcal{J} = 89.31\%$ for the (3+1)D spatiotemporal SM, and $\eta = 90.32\%$, $\mathcal{J} = 97.48\%$, and $\eta\mathcal{J} = 88.05\%$ for the vortex molecule.

The strength of the nonlocal Kerr nonlinearity has a significant effect on the quality of the optical memory. Figure 7c shows fidelity $\eta\mathcal{J}$ of the retrieved (3+1)D spatiotemporal SM as a function of the probe-pulse amplitude. For this purpose, a set of probe-pulse isosurfaces, $|\Omega_p\tau_0| = 3$, 11, and 19 at $z = 8L_{\rm diff} \approx 7$ mm are displayed. For the moderate amplitude, $|\Omega_p\tau_0| \approx 11$, the fidelity reaches its maximum, with the retrieved spatiotemporal SM having nearly the same shape as the original one prior to the storage. For small and large amplitudes, the fidelity features small values, that is, the retrieved SM is distorted greatly. This happens because, for the weak and strong probe-pulse amplitudes, the Kerr nonlinearity is either too weak or too strong to balance the diffraction and dispersion.

The nonlocality degree of the Kerr nonlinearity also has a significant effect on the memory quality for the spatiotemporal SMs. Figure 7d shows fidelity $\eta\mathcal{J}$ of the retrieved (3+1)D SM as a function of the nonlocality degree, σ. The probe-pulse isosurfaces ($|\Omega_p\tau_0| = 0.5$) are displayed for $\sigma = 0.5$, 1.4, and 5.0 at $z = 8L_{\rm diff} \approx 7$ mm. The fidelity reaches its maximum in the case of the moderate nonlocality degree, $\sigma \approx 1.4$, letting the retrieved SM keep nearly the same shape as the original one had. In the cases of small and large nonlocality degrees, the fidelity may have only small values, greatly distorting the retrieved SM. This happens because, in the limit of local response ($\sigma \to 0$), the Kerr nonlinearity becomes local, making all (3+1)D solitons unstable, as mentioned above. On the other hand, in the limit of the strongly nonlocal response ($\sigma \to \infty$), the nonlocal Kerr nonlinearity reduces to a linear potential (as in the above-mentioned "accessible-soliton" model[98]), which cannot support stable (3+1)D SMs either.

5. Conclusion

We have elaborated a scheme which makes it possible to create stable optical multidimensional SMs (soliton molecules), that is, bound states of zero-vorticity solitons, as well as bound states of vortex solitons, in a gas of cold Rydberg atoms, in which the laser illumination maintains the EIT setting. Due to the interplay of EIT and strong long-range Rydberg–Rydberg interaction between atoms, the system gives rise to giant nonlocal Kerr nonlinearity, which provides for the stability of the (2+1)D SMs (that would be completely unstable under the action of the local nonlinearity). The SMs feature large sizes, low generation powers, and can be effectively controlled by means of the nonlocality degree of the Kerr nonlinearity. The system allows, as well, the creation of stable (3+1)D spatiotemporal SMs, including those built of vortex spatiotemporal solitons, moving with ultraslow velocities and requiring very low generation powers. Further, the spatiotemporal solitons can be stored and retrieved through switching off and on of the control laser field. The findings reported here provide insight into the use of long-range atomic interactions for creating robust bound states of solitons and developing methods to effectively control them. The predictions reported here are helpful for experimental observations of high-dimensional soliton molecules and promising to find applications to optical data processing and transmission.

Supporting Information

Supporting Information is available from the Wiley Online Library or from the author.

Acknowledgements

The authors thank J. Peng for useful discussions. G.H. and C.H. acknowledge the support from National Natural Science Foundation of China (No. 11975098 and No. 11974117); C.H. acknowledges the support from National Key Research and Development Program of China (No. 2017YFA0304201); Shanghai Municipal Science and Technology Major Project (No. 2019SHZDZX01); B.A.M. acknowledges the support Israel Science Foundation (1286/17).

Conflict of Interest

The authors declare no conflict of interest.

Data Availability Statement

The data that support the findings of this study are available from the corresponding author upon reasonable request.

Keywords

nonlocal Kerr nonlinearity, Rydberg atoms, soliton molecules

Received: June 2, 2021
Revised: November 18, 2021
Published online:

[1] V. E. Zakharov, S. V. Manakov, S. P. Novikov, L. P. Pitaevskii, *Theory of Solitons: The Inverse Problem Method*, Nauka Publishers, Moscow **1980**.
[2] M. J. Ablowitz, H. Segur, *Solitons and the Inverse Scattering Transform*, SIAM, Philadelphia **1981**.
[3] E. A. Kuznetsov, A. M. Rubenchik, V. E. Zakharov, *Phys. Rep.* **1986**, *142*, 103.
[4] W. E. Torruellas, S. Trillo, *Spatial Solitons*, Springer Verlag, Berlin **2001**.
[5] A. Hasegawa, M. Matsumoto, *Optical Solitons in Fibers*, Springer, Berlin **2002**.
[6] Y. S. Kivshar, G. P. Agrawal, *Optical Solitons: From Fibers to Photonic Crystals*, Academic Press, Cambridge, MA **2003**.
[7] N. Akhmediev, A. Ankiewicz, *Dissipative Solitons*, Springer, Berlin **2005**.
[8] B. A. Malomed, *Soliton Management in Periodic Systems*, Springer Science & Business Media, Berlin **2006**.
[9] F. Lederer, G. I. Stegeman, D. N. Christodoulides, G. Assanto, M. Segev, Y. Silberberg, *Phys. Rep.* **2008**, *463*, 1.
[10] M. Wadati, *Eur. Phys. J. Spec. Top.* **2009**, *173*, 223.
[11] A. I. Maimistov, *Quantum Electron.* **2010**, *40*, 756.
[12] S. K. Turitsyn, B. G. Bale, M. P. Fedoruk, *Phys. Rep.* **2012**, *521*, 135.

[13] P. Grelu, N. Akhmediev, *Nat. Photonics* **2012**, *6*, 84.
[14] G. Assanto, *Nematicons: Spatial Optical Solitons in Nematic Liquid Crystals*, Wiley, Hoboken, NJ **2012**.
[15] V. A. Brazhnyi, V. V. Konotop, *Mod. Phys. Lett.* **2004**, *18*, 627.
[16] F. K. Abdullaev, A. Gammal, A. M. Kamchatnov, L. Tomio, *Int. J. Mod. Phys. B* **2005**, *19*, 3415.
[17] D. J. Frantzeskakis, *J. Phys. A: Math. Theor.* **2010**, *43*, 213001.
[18] L. Salasnich, *Opt. Quantum Electron.* **2017**, *49*, 409.
[19] A. V. Ustinov, *Solitons in Josephson Junctions: Physics of Magnetic Fluxons in Superconducting Junctions and Arrays*, Wiley, Hoboken, NJ **2005**.
[20] T. Dauxois, M. Peyrard, *Physics of Solitons*, Cambridge University Press, Cambridge **2006**.
[21] P. G. Kevrekidis, *The Discrete Nonlinear Schrödinger Equation: Mathematical Analysis, Numerical Computations, and Physical Perspectives*, Springer, Berlin **2009**.
[22] Y. V. Kartashov, B. A. Malomed, L. Torner, *Rev. Mod. Phys.* **2011**, *83*, 247.
[23] F. D. Tappert, N. J. Zabusky, *Phys. Rev. Lett.* **1971**, *27*, 1774.
[24] Y. S. Kivshar, B. A. Malomed, *Rev. Mod. Phys.* **1989**, *61*, 763.
[25] V. Tikhonenko, J. Christou, B. Luther-Davies, *Phys. Rev. Lett.* **1996**, *76*, 2698.
[26] W. Krolikowski, S. A. Holmstrom, *Opt. Lett.* **1997**, *22*, 369.
[27] W. Krolikowski, B. Luther-Davies, C. Denz, T. Tschudi, *Opt. Lett.* **1998**, *23*, 97.
[28] S. Gatz, J. Herrmann, *IEEE J. Quantum Electron.* **1992**, *28*, 1732.
[29] F. Lu, Q. Lin, W. H. Knox, G. P. Agrawal, *Phys. Rev. Lett.* **2004**, *93*, 183901.
[30] J. Pfeiffer, M. Schuster, A. A. Abdumalikov, Jr, A. V. Ustinov, *Phys. Rev. Lett.* **2006**, *96*, 034103.
[31] J. H. V. Nguyen, P. Dyke, D. Luo, B. A. Malomed, R. G. Hulet, *Nat. Phys.* **2014**, *10*, 918.
[32] O. Descalzi, J. Cisternas, D. Escaff, H. R. Brand, *Phys. Rev. Lett.* **2009**, *102*, 188302.
[33] M. D. Maiden, L. D. Bookman, M. A. Hoefer, *Phys. Rev. B* **2014**, *89*, 180409(R).
[34] F. Köttig, F. Tani, J. C. Travers, P. S. J. Russell, *Phys. Rev. Lett.* **2017**, *118*, 263902.
[35] O. Descalzi, H. R. Brand, *Phys. Rev. E* **2020**, *101*, 040201(R).
[36] B. A. Malomed, *Phys. Rev. A* **1991**, *44*, 6954.
[37] B. A. Malomed, *Phys. Rev. A* **1993**, *47*, 2874.
[38] B. A. Malomed, A. A. Nepomnyashchy, *Europhys. Lett.* **1994**, *27*, 649.
[39] B. A. Malomed, *Europhys. Lett.* **1995**, *30*, 507.
[40] V. V. Afanasjev, B. A. Malomed, P. L. Chu, *Phys. Rev. E* **1997**, *56*, 6020.
[41] D. Y. Tang, W. S. Man, H. Y. Tam, P. D. Drummond, *Phys. Rev. A* **2001**, *64*, 033814.
[42] D. Y. Tang, B. Zhao, L. M. Zhao, H. Y. Tam, *Phys. Rev. E* **2005**, *72*, 016616.
[43] A. Komarov, K. Komarov, F. Sanchez, *Phys. Rev. A* **2009**, *79*, 033807.
[44] Y. Wang, F. Leo, J. Fatome, M. Erkintalo, S. G. Murdoch, S. Coen, *Optica* **2017**, *4*, 855.
[45] H. Sakaguchi, D. V. Skryabin, B. A. Malomed, *Opt. Lett.* **2018**, *43*, 2688.
[46] A. Gelash, D. Agafontsev, V. Zakharov, G. El, S. Randoux, P. Suret, *Phys. Rev. Lett.* **2019**, *123*, 234102.
[47] N. N. Akhmediev, A. Ankiewicz, *Phys. Rev. Lett.* **1998**, *79*, 4047.
[48] L.-C. Crasovan, Y. V. Kartashov, D. Mihalache, L. Torner, Y. S. Kivshar, V. M. Pérez-García, *Phys. Rev. E* **2003**, *67*, 046610.
[49] V. M. Pérez-García, V. Vekslerchik, *Phys. Rev. E* **2003**, *67*, 061804.
[50] M. Stratmann, T. Pagel, F. Mitschke, *Phys. Rev. Lett.* **2005**, *95*, 143902.
[51] A. Hause, H. Hartwig, M. Böhm, F. Mitschke, *Phys. Rev. A* **2008**, *78*, 063817.
[52] A. Haboucha, H. Leblond, M. Salhi, A. Komarov, F. Sanchez, *Opt. Lett.* **2008**, *33*, 524.
[53] A. Zavyalov, R. Iliew, O. Egorov, F. Lederer, *Phys. Rev. A* **2009**, *80*, 043829.
[54] U. A. Khawaja, *Phys. Rev. E* **2010**, *81*, 056603.
[55] C. Yin, N. G. Berloff, V. M. Pérez-García, D. Novoa, A. V. Carpentier, H. Michinel, *Phys. Rev. A* **2011**, *83*, 051605(R).
[56] U. A. Khawaja, H. T. C. Stoof, *New J. Phys.* **2011**, *13*, 085003.
[57] K. Lakomy, R. Nath, L. Santos, *Phys. Rev. A* **2012**, *86*, 013610.
[58] P. Rohrmann, A. Hause, F. Mitschke, *Phys. Rev. A* **2013**, *87*, 043834.
[59] A. Boudjemâa, U. A. Khawaja, *Phys. Rev. A* **2013**, *88*, 045801.
[60] A. Hause, F. Mitschke, *Phys. Rev. A* **2013**, *88*, 063843.
[61] W. E. Shirley, B. M. Anderson, C. W. Clark, R. M. Wilson, *Phys. Rev. Lett.* **2014**, *113*, 165301.
[62] S. M. Alamoudi, U. A. Khawaja, B. B. Baizakov, *Phys. Rev. A* **2014**, *89*, 053817.
[63] B. K. Turmanov, B. B. Baizakov, B. A. Umarov, F. K. Abdullaev, *Phys. Lett. A* **2015**, *379*, 1828.
[64] B. B. Baizakov, S. M. Al-Marzoug, H. Bahlouli, *Phys. Rev. A* **2015**, *92*, 033605.
[65] A. Niang, F. Amrani, M. Salhi, H. Leblond, F. Sanchez, *Phys. Rev. A* **2015**, *92*, 033831.
[66] P. Wang, C. Bao, B. Fu, X. Xiao, P. Grelu, C. Yang, *Opt. Lett.* **2016**, *41*, 2254.
[67] G. Herink, F. Kurtz, B. Jalali, D. R. Solli, C. Ropers, *Science* **2017**, *356*, 50.
[68] K. Krupa, K. Nithyanandan, U. Andral, P. Tchofo-Dinda, P. Grelu, *Phys. Rev. Lett.* **2017**, *118*, 243901.
[69] Y. Luo, J. Cheng, B. Liu, Q. Sun, L. Li, S. Fu, D. Tang, L. Zhao, D. Liu, *Sci. Rep.* **2017**, *7*, 2369.
[70] X. Liu, X. Yao, Y. Cui, *Phys. Rev. Lett* **2018**, *121*, 023905.
[71] H. Qin, X. Xiao, P. Wang, C. Yang, *Opt. Lett.* **2018**, *43*, 1982.
[72] J. Peng, H. Zeng, *Laser Photonics Rev.* **2018**, *12*, 1800009.
[73] G. Xu, A. Gelash, A. Chabchoub, V. Zakharov, B. Kibler, *Phys. Rev. Lett.* **2019**, *122*, 084101.
[74] O. Melchert, S. Willms, S. Bose, A. Yulin, B. Roth, F. Mitschke, U. Morgner, I. Babushkin, A. Demircan, *Phys. Rev. Lett.* **2019**, *123*, 243905.
[75] Z. Q. Wang, K. Nithyanandan, A. Coillet, P. Tchofo-Dinda, P. Grelu, *Nat. Commun.* **2019**, *10*, 830.
[76] Y. Zhou, Y.-X. Ren, J. Shi, H. Mao, K. K. Y. Wong, *Optica* **2020**, *7*, 965.
[77] F. Kurtz, C. Ropers, G. Herink, *Nat. Photonics* **2020**, *14*, 9.
[78] W. Weng, R. Bouchand, E. Lucas, E. Obrzud, T. Herr, T. J. Kippenberg, *Nat. Commun.* **2020**, *11*, 2402.
[79] A. Maître, G. Lerario, A. Medeiros, F. Claude, Q. Glorieux, E. Giacobino, S. Pigeon, A. Bramati, *Phys. Rev. X* **2020**, *10*, 041028.
[80] L. Bergé, *Phys. Rep.* **1998**, *303*, 259.
[81] C. Sulem, P.-L. Sulem, *The Nonlinear Schrödinger Equation: Self-Focusing and Wave Collapse*, Springer, Berlin **1999**.
[82] B. A. Malomed, D. Mihalache, F. Wise, L. Torner, *J. Opt. B: Quantum Semiclassical Opt.* **2005**, *7*, R53.
[83] G. Fibich, *The Nonlinear Schrödinger Equation: Singular Solutions and Optical Collapse*, Springer, Berlin **2015**.
[84] M. Quiroga-Teixeiro, H. Michinel, *J. Opt. Soc. Am. B* **1997**, *14*, 2004.
[85] R. L. Pego, H. A. Warchall, *J. Nonlinear Sci.* **2002**, *12*, 347.
[86] B. A. Malomed, *Phys. D* **2019**, *399*, 108.
[87] B. A. Malomed, *Eur. Phys. J. Spec. Top.* **2016**, *225*, 2507.
[88] Y. V. Kartashov, G. E. Astrakharchik, B. A. Malomed, L. Torner, *Nat. Rev. Phys.* **2019**, *1*, 185.
[89] E. Kengne, W.-M. Liu, B. A. Malomed, *Phys. Rep.* **2021**, *899*, 1.
[90] E. L. Falcao-Filho, C. B. de Araújo, G. Boudebs, H. Leblond, V. Skarka, *Phys. Rev. Lett.* **2013**, *110*, 013901.
[91] C. R. Cabrera, L. Tanzi, J. Sanz, B. Naylor, P. Thomas, P. Cheiney, L. Tarruell, *Science* **2018**, *359*, 301.

[92] P. Cheiney, C. R. Cabrera, J. Sanz, B. Naylor, L. Tanzi, L. Tarruell, *Phys. Rev. Lett.* **2018**, *120*, 135301.
[93] G. Semeghini, G. Ferioli, L. Masi, C. Mazzinghi, L. Wolswijk, F. Minardi, M. Modugno, G. Modugno, M. Inguscio, M. Fattori, *Phys. Rev. Lett.* **2018**, *120*, 235301.
[94] C. D'Errico, A. Burchianti, M. Prevedelli, L. Salasnich, F. Ancilotto, M. Modugno, F. Minardi, C. Fort, *Phys. Rev. Res.* **2019**, *1*, 033155.
[95] F. Böttcher, J.-N. Schmidt, J. Hertkorn, K. S. H. Ng, S. D. Graham, M. Guo, T. Langen, T. Pfau, *Rep. Prog. Phys.* **2020**, *84*, 012403.
[96] Z. Luo, W. Pang, B. Liu, Y. Li, B. A. Malomed, *Front. Phys.* **2021**, *16*, 32201.
[97] A. S. Reyna, G. Boudebs, B. A. Malomed, C. B. de Araújo, *Phys. Rev. A* **2016**, *93*, 013840.
[98] A. W. Snyder, D. J. Mitchell, *Science* **1997**, *276*, 1538.
[99] W. Królikowski, *Phys. Rev. E* **2000**, *63*, 016610.
[100] C. Conti, M. Peccianti, G. Assanto, *Phys. Rev. Lett.* **2004**, *92*, 113902.
[101] Z. Xu, Y. V. Kartashov, L. Torner, *Phys. Rev. Lett.* **2005**, *95*, 113901.
[102] A. Alberucci, M. Peccianti, G. Assanto, A. Dyadyusha, M. Kaczmarek, *Phys. Rev. Lett.* **2006**, *97*, 153903.
[103] D. Buccoliero, A. S. Desyatnikov, W. Krolikowski, Y. S. Kivshar, *Phys. Rev. Lett.* **2007**, *98*, 053901.
[104] S. Skupin, M. Saffman, W. Królikowski, *Phys. Rev. Lett.* **2007**, *98*, 263902.
[105] I. B. Burgess, M. Peccianti, G. Assanto, R. Morandotti, *Phys. Rev. Lett.* **2009**, *102*, 203903.
[106] C. Conti, M. A. Schmidt, P. S. J. Russell, F. Biancalana, *Phys. Rev. Lett.* **2010**, *105*, 263902.
[107] F. Maucher, N. Henkel, M. Saffman, W. Królikowski, S. Skupin, T. Pohl, *Phys. Rev. Lett.* **2011**, *106*, 170401.
[108] S. Sevinçli, N. Henkel, C. Ates, T. Pohl, *Phys. Rev. Lett.* **2011**, *107*, 153001.
[109] O. Lahav, O. Kfir, P. Sidorenko, M. Mutzafi, A. Fleischer, O. Cohen, *Phys. Rev. X* **2017**, *7*, 041051.
[110] T. P. Horikis, D. J. Frantzeskakis, *Phys. Rev. Lett.* **2017**, *118*, 243903.
[111] B.-X. Li, V. Borshch, R.-L. Xiao, S. Paladugu, T. Turiv, S. V. Shiyanovskii, O. D. Lavrentovich, *Nat. Commun.* **2018**, *9*, 2912.
[112] K. E. Wilson, N. Westerberg, M. Valiente, C. W. Duncan, E. M. Wright, P. Öhberg, D. Faccio, *Phys. Rev. Lett.* **2018**, *121*, 133903.
[113] Z. Bai, W. Li, G. Huang, *Optica* **2019**, *6*, 309.
[114] C. Rotschild, B. Alfassi, O. Cohen, M. Segev, *Nat. Phys.* **2006**, *2*, 769.
[115] I. Tikhonenkov, B. A. Malomed, A. Vardi, *Phys. Rev. Lett.* **2008**, *100*, 090406.
[116] M. Fleischhauer, A. Imamoglu, J. P. Marangos, *Rev. Mod. Phys.* **2005**, *77*, 633.
[117] T. F. Gallagher, *Rydberg Atoms*, Cambridge University Press, Cambridge **2008**.
[118] M. Saffman, T. G. Walker, K. Mølmer, *Rev. Mod. Phys.* **2010**, *82*, 2313.
[119] C. S. Adams, J. D. Pritchard, J. P. Shaffer, *J. Phys. B: At. Mol. Opt. Phys.* **2020**, *53*, 012002.
[120] O. Firstenberg, C. S. Adams, S. Hofferberth, *J. Phys. B: At. Mol. Opt. Phys.* **2016**, *49*, 152003.
[121] C. Murray, T. Pohl, *Adv. At., Mol., Opt. Phys.* **2016**, *65*, 321.
[122] Z. Bai, G. Huang, *Opt. Express* **2016**, *24*, 4442.
[123] H. Busche, P. Huillery, S. W. Ball, T. Ilieva, M. P. A. Jones, C. S. Adams, *Nat. Phys.* **2017**, *13*, 655.
[124] Here $k_1 = 0$, $k_2 = k_p$, and $k_3 = k_p + k_c$. In the Schrödinger picture, $\hat{\sigma}_{\alpha\beta}(z) \equiv |\alpha\rangle_{zz}\langle\beta|$, where $|\alpha\rangle_z$ is energy eigenstate $|\alpha\rangle$ of the atom located at position z.
[125] Y. Mu, L. Qin, Z. Shi, G. Huang, *Phys. Rev. A* **2021**, *103*, 043709.
[126] Here "2" pertains to the transverse coordinates, ξ and η, while "1" refers to the evolution coordinate, ζ.
[127] B. A. Malomed, *Phys. Rev. E* **1998**, *58*, 7928.
[128] S. Raghavan, G. P. Agrawal, *Opt. Commun.* **2000**, *180*, 377.
[129] B. A. Malomed, *Prog. Opt.* **2002**, *43*, 71.
[130] P. Schauß, M. Cheneau, M. Endres, T. Fukuhara, S. Hild, A. Omran, T. Pohl, C. Gross, S. Kuhr, I. Bloch, *Nature* **2012**, *491*, 87.
[131] Such soliton molecules can be generated experimentally. For example, to obtain a 2D spatial soliton molecule consisting of two spatial solitons, one needs first to prepare two solitons at the entrance of the Rydberg gas. Then, the solitons are incident to the Rydberg gas with a proper space separation and initial velocities. The initial velocity of each soliton is acquired when the soliton is incident obliquely. The relation between the soliton velocity v and the incidence angle θ is given by $\theta = \arctan(v)$.
[132] D. Buccoliero, A. S. Desyatnikov, W. Krolikowski, Y. S. Kivshar, *Phys. Rev. Lett.* **2007**, *98*, 053901.
[133] K. E. Strecker, G. B. Partridge, A. G. Truscott, R. G. Hulet, *New J. Phys.* **2003**, *5*, 73.
[134] Here "3" pertains to the transverse and temporal coordinates, ξ, η, and τ, respectively, while "1" refers to the evolution coordinate, ζ.
[135] M. Fleischhauer, M. D. Lukin, *Phys. Rev. Lett.* **2000**, *84*, 5094.
[136] C. Liu, Z. Dutton, C. H. Behroozi, L. V. Hau, *Nature* **2001**, *409*, 490.
[137] D. F. Phillips, A. Fleischhauer, A. Mair, R. L. Walsworth, M. D. Lukin, *Phys. Rev. Lett.* **2001**, *86*, 783.
[138] M. Shuker, O. Firstenberg, R. Pugatch, A. Ron, N. Davidson, *Phys. Rev. Lett.* **2008**, *100*, 223601.
[139] I. Novikova, R. L.Walsworth, Y. Xiao, *Laser Photonics Rev.* **2012**, *6*, 333.
[140] Y.-H. Chen, M.-J. Lee, I.-C. Wang, S. Du, Y.-F. Chen, Y.-C. Chen, I. A. Yu, *Phys. Rev. Lett.* **2013**, *110*, 083601.
[141] D. Maxwell, D. J. Szwer, D. Paredes-Barato, H. Busche, J. D. Pritchard, A. Gauguet, K. J. Weatherill, M. P. A. Jones, C. S. Adams, *Phys. Rev. Lett.* **2013**, *110*, 103001.
[142] Y. O. Dudin, L. Li, A. Kuzmich, *Phys. Rev. A* **2013**, *87*, 031801(R).
[143] G. Heinze, C. Hubrich, T. Halfmann, *Phys. Rev. Lett.* **2013**, *111*, 033601.
[144] Y. Chen, Z. Bai, G. Huang, *Phys. Rev. A* **2014**, *89*, 023835.
[145] N. Šibalić, J. M. Kondo, C. S. Adams, K. J. Weatherill, *Phys. Rev. A* **2016**, *94*, 033840.
[146] Y.-F. Hsiao, P.-J. Tsai, H.-S. Chen, S.-X. Lin, C.-C. Hung, C.-H. Lee, Y.-H. Chen, Y.-F. Chen, I.-A. Yu, Y.-C. Chen, *Phys. Rev. Lett.* **2018**, *120*, 183602.
[147] A. B. Matsko, Y. V. Rostovtsev, O. Kocharovskaya, A. S. Zibrov, M. O. Scully, *Phys. Rev. A* **2001**, *64*, 043809.